Atomic and Electronic Structure of Ultrathin Bi(111) Films Grown on Bi_2Te_3(111) Substrates: Evidence for a Strain-Induced Topological Phase Transition

T. Hirahara,[1,*] N. Fukui,[1] T. Shirasawa,[2] M. Yamada,[1] M. Aitani,[1] H. Miyazaki,[3] M. Matsunami,[3] S. Kimura,[3] T. Takahashi,[2] S. Hasegawa,[1] and K. Kobayashi[4]

[1]*Department of Physics, University of Tokyo, 7-3-1 Hongo, Bunkyo-ku, Tokyo 113-0033, Japan*
[2]*Institute for Solid State Physics, University of Tokyo, 5-1-5 Kashiwanoha, Kashiwa 277-8581, Japan*
[3]*UVSOR Facility, Institute for Molecular Science, Okazaki 444-8585, Japan*
[4]*Department of Physics, Ochanomizu University, 2-1-1 Otsuka, Bunkyo-ku, Tokyo 112-8610, Japan*

(Received 26 January 2012; revised manuscript received 10 September 2012; published 30 November 2012)

We studied the atomic and electronic structures of ultrathin Bi(111) films grown on Bi_2Te_3 by means of angle-resolved photoemission, first-principles calculations, and low-energy electron diffraction. These Bi films were found to be strained due to the influence of the substrate. Accordingly, the band structure is affected and Bi undergoes a topological phase transition; it is shown that the Z_2 topological invariant in three dimensions switches from $+1$ (trivial) to -1 (nontrivial or topological). This was clearly confirmed from the change in the surface-state dispersion near the Fermi level. Our discovery offers a method to produce novel topological systems from simple materials.

DOI: 10.1103/PhysRevLett.109.227401 PACS numbers: 78.66.Nk, 73.20.−r, 73.61.Ng, 75.70.Tj

Topological insulators have become one of the model systems to study Dirac physics in solids. They are mathematically characterized by the Z_2 topological number with edge modes that cannot be backscattered [1,2]. An essential ingredient in realizing a topological insulator is the parity inversion induced by the strong spin-orbit coupling. From this viewpoint, bismuth (Bi), which is virtually the heaviest nonradioactive element, has been the main building block. Nowadays not only binary ($Bi_{1-x}Sb_x$, Bi_2Te_3, or Bi_2Se_3 [3]) but also ternary ($TlBiSe_2$ [4]) or even quaternary alloys ($Bi_{2-x}Sb_xTe_{3-y}Se_y$ [5]) are known as topological insulators. Although it is necessary to make such complex structures which are bulk insulators, inhomogeneity may be introduced in the grown samples. Therefore, searching for other ways to produce novel topological materials with simple, well-defined structures is important.

In this respect, driving a quantum topological phase transition [making a normal (trivial) material into a topological (nontrivial) one] in a simple system seems to be a rather smart approach. One example of such a transition is the case of Bi, where the three-dimensional (3D) trivial bulk becomes topological in two dimensions by making thin films of 1–8 bilayers (BL) [6,7]. Another way is to apply pressure, which has been theoretically predicted for BiTeI [8], ternary Heusler [9], or antiperovskite compounds [10]. Additionally, $TlBi(S_{1-x}Se_x)_2$ is said to undergo a topological phase transition by changing x [11,12]. Still, these materials are quite complicated except for the case of Bi.

In the present Letter, we report on an unprecedented quantum topological phase transition in pure Bi triggered by strain. We fabricated ultrathin Bi films on a Bi_2Te_3 substrate and studied the atomic and electronic structures as well as calculated Z_2 invariants. We have found that the films have smaller in-plane and larger out-of-plane lattice constants compared to the bulk values. This distortion induced a clear change in the band dispersion of the surface and quantum-well states compared to that of the Bi films formed on Si(111)-(7×7), which have bulklike lattice parameters [13,14]. Furthermore, this strain was shown to switch the Z_2 topological number of bulk Bi from trivial to nontrivial. Thus, our results present a way to induce topological phases in simple systems.

The film fabrication and measurements were done *in situ*. First, a clean Si(111)-(7×7) surface was prepared by cycles of resistive heat treatments. Then Bi was deposited on the 7×7 structure at ~400 K under Te-rich conditions. Such a procedure is reported to result in a quintuple layer by quintuple layer (QL, 1 QL = 10.2 Å) epitaxial Bi_2Te_3(111) film growth [15]. Then, Bi was further deposited on the Bi_2Te_3 at room temperature [16]. The film coverage was carefully calibrated by the reflection high-energy electron diffraction oscillation period and cross-checked by other methods [17].

The angle-resolved photoemission spectroscopy (ARPES) experiments were performed at BL-5U of UVSOR-II using an MBS-Toyama A-1 analyzer at 10 K. The photon energy used was $h\nu = 21$ eV, and the energy and angular resolutions were 20 meV and 0.2 deg, respectively. The low-energy electron diffraction (LEED) spot intensity was acquired with a charge-coupled-device camera at 80 K. First-principles calculations were performed using the WIEN2K computer code on the basis of the augmented plane wave + local orbitals method taking into account the spin-orbit interaction, and the generalized gradient approximation [18] was used for the description of exchange-correlation potential.

Figure 1 shows the comparison of the band structure of ultrathin Bi(111) films formed on Bi_2Te_3(111) [raw ARPES intensity map (a) and its second derivative with respect to energy (c)] and on Si(111)-(7 × 7) (d), respectively, along the $\bar{\Gamma}$-$\bar{M}$ direction [Fig. 1(e)]. The film thickness is nearly the same (~ 7 BL). Since the photoemission intensity near $\bar{\Gamma}$ is much stronger than that near $\bar{M}$, it is almost impossible to see the fine structures near $\bar{M}$ in the raw data [19]. Also, the intensity drops significantly near E_F. But by taking the line profile of the image just below E_F (10 meV), we obtain a momentum distribution curve as shown in Fig. 1(b). It shows several peaks corresponding to bands crossing the Fermi level. In particular, a clear peak structure at 0.6 $Å^{-1}$ can be noticed, showing that indeed there are some states near $\bar{M}$. These bands can be seen better in Fig. 1(c). Therefore. we will use both the raw data and the second derivative images in the following discussion. While the basic features near the $\bar{M}$ point and that at 0.4–0.8 eV below the Fermi level (E_F) at $\bar{\Gamma}$ are quite similar between Figs. 1(c) and 1(d), there is one significant difference: the shallow surface-state electron pocket around $\bar{\Gamma}$ in (d) is replaced by hole bands that disperse linearly away from E_F in (c). This shows that although they are the same "Bi" films with nearly the same film thickness, they are not identical.

It is known that the structure of the Bi(111) films on Si(111)-(7 × 7) system is bulklike (only small deviation from the bulk lattice constant) [14,17] and its band dispersion is reproduced by the calculation for a freestanding slab [13], meaning that the substrate has minimal effects. However, since the lattice constant of Bi_2Te_3(111) is 4.38 Å, which is 3.6% smaller than that of Bi(111) (4.54 Å), the atomic structure may be altered and change the electronic structure discussed above. To check this hypothesis, we have performed LEED *I-V* analysis on the 6 BL Bi/20 QL Bi_2Te_3(111) system. Figure 2(a) shows the measured *I-V* curves (solid lines) for various diffraction spots. A LEED pattern taken at 100 eV is shown in the inset. As a comparison, the *I-V* curve for the Bi/Si system is shown together for the {1, 0} spot [20], clearly indicating that it is different from that of Bi/Bi_2Te_3. The theoretical *I-V* spectra were calculated on the basis of the dynamical diffraction theory using the Barbieri–van Hove symmetrized automated tensor LEED package [21]. The in-plane lattice constant was determined from the positions of the LEED spots to be 4.39 ± 0.05 Å (− 3.3% compared to the bulk value). The optimized structure with the Debye temperatures is depicted in Fig. 2(b) [22]. The experimental and theoretical *I-V* spectra [dotted lines in Fig. 2(a)] agree very well (Pendry *R* factor is 0.172 ± 0.026). The Debye temperature of the topmost bilayer Bi is 70 and 90 K, lower than that for the bulk (140 K). This is consistent with that for the single crystal Bi(111) surface [23]. In summary, we can say that the average intrabilayer Bi distance is 1.64 ± 0.04 Å, and the interbilayer distance is 2.42 ± 0.04 Å. Compared to the bulk values (1.59 and 2.34 Å) they are

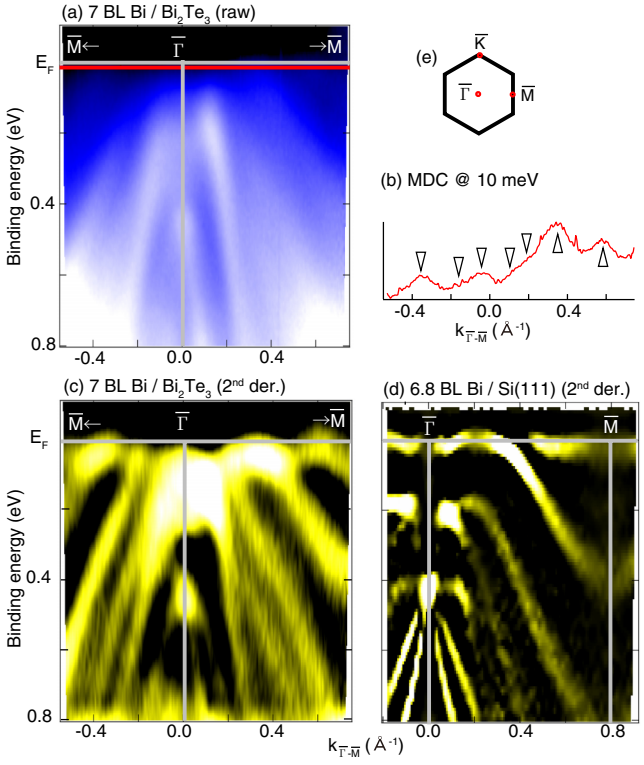

FIG. 1 (color online). (a) Raw ARPES band dispersion image of a 7 BL Bi(111) ultrathin film formed on Bi_2Te_3(111). (b) Momentum distribution curve at 10 meV below the Fermi level [red horizontal solid line in (a)]. (c) Second derivative with respect to energy of (a). (d) Band dispersion of a 6.8 BL ultrathin Bi(111) film formed on Si(111)-(7 × 7). (e) Surface Brillouin zone of Bi(111). The bright color represents high intensity.

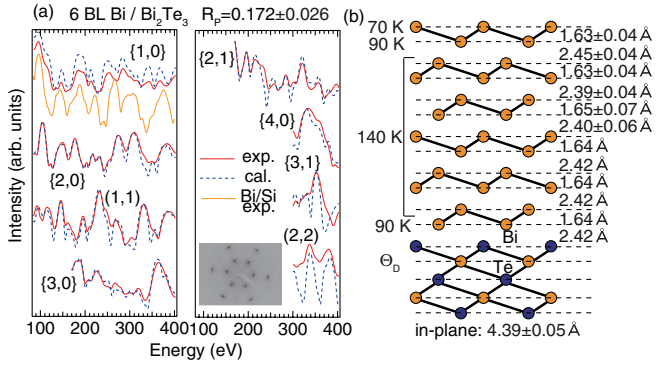

FIG. 2 (color online). (a) Experimental *I-V* spectra of LEED spots at 80 K for the 6 BL Bi(111) ultrathin film formed on Bi_2Te_3 and the calculated spectra of the optimized model shown in (b). The *I-V* curve for the Bi(111) ultrathin film formed on Si(111)-(7 × 7) is shown for the {1, 0} spot. The inset shows the LEED pattern at 100 eV. (b) Cross-sectional view of the optimized model of the 6 BL Bi(111) film on Bi_2Te_3. The Debye temperature for each layer is also shown.

expanded by 3.1 and 3.4%, respectively. This model has also been confirmed by surface X-ray diffraction measurements [24].

Now we turn to the comparison of the ARPES and first-principles calculations. We have performed band structure calculations for freestanding Bi slabs with the in-plane lattice constant fixed to 4.38 Å. The out-of-plane lattice parameters in the calculation were optimized by minimizing the total energy of the system, and the average intrabilayer Bi distance is 1.70 ± 0.02 Å (+ 6.9% compared to bulk) and the interbilayer distance is 2.40 ± 0.02 Å (+ 2.6%). These values are in reasonable agreement with those estimated experimentally [Fig. 2(b)].

For the 1–4 BL thick Bi(111) films formed on Bi_2Te_3, the agreement between experiment and calculation was rather poor since the substrate effect should be important in the very thin films (Fig. S1 in Supplemental Material [25]) [16]. Figures 3(a) and 3(b) [3(d) and 3(e)] are the experimentally obtained band dispersion images for the 5 BL [6 BL] Bi(111) film on Bi_2Te_3. Shown in Figs. 3(c) and 3(f) is the weighed spectral function (WSF), which is calculated as $\mathrm{WSF}(E,k) = \Sigma_n \delta(E - \epsilon_n(k)) w_n(k)$, where $\epsilon_n(k)$ is the energy in the n-th band at wave vector k and $w_n(k)$ is its magnitude of the wave function localization to the topmost surface bilayer. In the actual calculation, $\delta(x)$ is replaced by $(1/\pi)[\Delta/(x^2 + \Delta^2)]$ ($\Delta = 0.1$ eV) to simulate the broadening effect. We have adopted WSF because the photoemission measurement is quite surface sensitive and not all the states in the calculation can be detected, as will be shown later. From Figs. 3(a)–3(f), we can say that there is a reasonable agreement between the experimental data and theory.

Looking more carefully, the states near $\bar{\Gamma}$ in the vicinity of E_F are quantum-well states (QWS) showing thickness dependence. The two states that are close to E_F near $\bar{M}$ do not show significant thickness dependence and are likely surface states (SS A). Compared to the calculation, the dispersion is rather flat for the state closest to E_F. There is another surface state (SS B), which is located at ~0.4–0.5 eV near the $\bar{\Gamma}$ point. The dispersion is a typical Rashba-type in both the experiment and the calculation, but the exact energy position is somewhat different. These slight differences can be adjusted by changing the lattice parameters. In Fig. 3(g), we have plotted the WSF for the 6 BL Bi film using the lattice constants determined from the LEED I-V measurements. While the band closer to

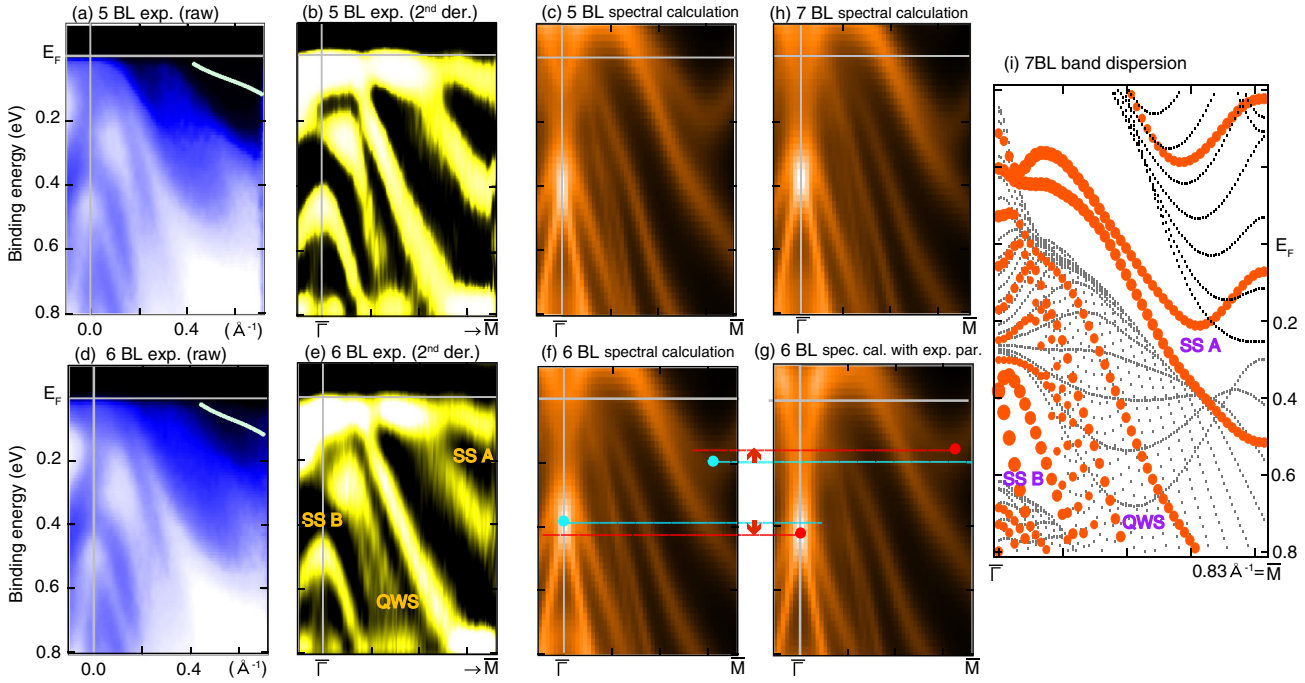

FIG. 3 (color online). (a) Experimentally measured raw ARPES image along the $\bar{\Gamma}$-$\bar{M}$ direction of the 5 BL ultrathin Bi(111) film on Bi_2Te_3, and its second derivative with respect to energy (b), to highlight the spectral features. (c) The calculated weighed spectral function (WSF) for a 5 BL strained Bi(111) ultrathin film, which is the band dispersion weighed by the magnitude of the wave function localization at the topmost Bi bilayer. (d) Experimentally measured raw ARPES image along the $\bar{\Gamma}$-$\bar{M}$ direction of the 6 BL Bi(111) film on Bi_2Te_3, and its second derivative with respect to energy (e). [(f) and (g)] The WSF for a 6 BL strained Bi(111) film. In (f), the optimized structure in the calculation is used, whereas in (g) the experimentally obtained lattice parameters are used. The arrows show the slight energy change. (h) The WSF for a 7 BL strained Bi(111) film. (i) The band dispersion for the 7 BL strained Bi(111) film together with the bulk band projection. The size of the circles represents the magnitude of the surface localization of the wave function. SS and QWS represent surface and quantum-well states, respectively.

E_F of SS A moves towards the Fermi level showing less dispersion, SS B moves to a slightly higher binding energy, and the agreement between theory and experiment improves [26].

Figure 3(h) shows the WSF for the 7 BL film, which agrees nicely with Figs. 1(a) and 1(c). Figure 3(i) is the actual band dispersion of the 7 BL film (the size of the markers shows the magnitude of the surface localization). Shown together is the bulk band projection, and the SS and QWS can be distinguished clearly. We should note that there are actually many states just below E_F near $\bar{\Gamma}$, which was not so clearly seen in the ARPES data and WSF image. We believe that since $w_n(k)$ for these states is not so large, there are not enough photoemitted electrons to actually resolve them clearly.

We proceed to the calculation of the Z_2 topological number using the "parity method" [27] as in Ref. [7]. First, we calculate the Z_2 number ν in two dimensions for the thin films by multiplying the parity of the occupied bands at the $\bar{\Gamma}$ and $\bar{M}$ points [time-reversal invariant points, Fig. 1(e)]. The calculated band dispersion is shown in Figs. 3 and S2 and the deduced parity is summarized in Table S1 (Supplemental Material [25]). The result is the same as that shown in Ref. [7] for bulklike films, and all the films are nontrivial.

Next, we calculate the Z_2 number in 3D bulk. In this case, there are four topological numbers: (ν_0; ν_1 ν_2 ν_3). To calculate ν_0, the multiplication of the parity of the occupied bands at the time-reversal invariant points Γ, L, X, and T [Fig. 4(a)] is performed. Figures 4(b) and 4(c) show the 3D Bi bulk band dispersion assuming the in-plane lattice constant of 4.38 and 4.54 Å, respectively. Both are semimetals with a hole pocket at T and an electron pocket at L. However, the Fermi wave number is larger for the 4.38 Å case (b). Focusing on ν_0, Bi is trivial with $\nu_0 = 0$ [27] for the usual bulk lattice constant of 4.54 Å. When the lattice constant is distorted, a band inversion takes place at the L point; the occupied and unoccupied states closest to E_F reverse as well as the bands below them [Fig. 4(b)]. As a consequence, the parity multiplication changes its sign at the L point. Since this does not occur at Γ, X, and T points, ν_0 changes its sign accordingly; a topological phase transition occurs and thus strained Bi becomes nontrivial. This can also be recognized in its edge state dispersion. While one of the surface states in Fig. 3(i) connects to the valence bands at both $\bar{\Gamma}$ and $\bar{M}$, the other one connects to the valence band at the $\bar{\Gamma}$ point and the conduction band at the $\bar{M}$ point, a characteristic feature of the topological edge states. Therefore, it becomes a topological semimetal such as Sb [27]. The tight-binding calculation based on the transfer-matrix method [28] for the two lattice constants clearly shows the change in the edge state dispersion from trivial to nontrivial [Fig. 4(f)], where the parameters have been determined by fitting to the band structures calculated by a density-functional method]. By comparison of Figs. 3(i) and 4(f), it can be said that the surface states of the 7 BL film have the same band dispersion as that of the semi-infinite films (bulk). It is now well conceptualized that utilizing ultrathin films is a powerful method to investigate the peculiar nature of the topological surface states [29]. Similarly, the peculiar topological properties, such as the step transmission properties of Sb surface states [30], should be observable using these strained Bi films.

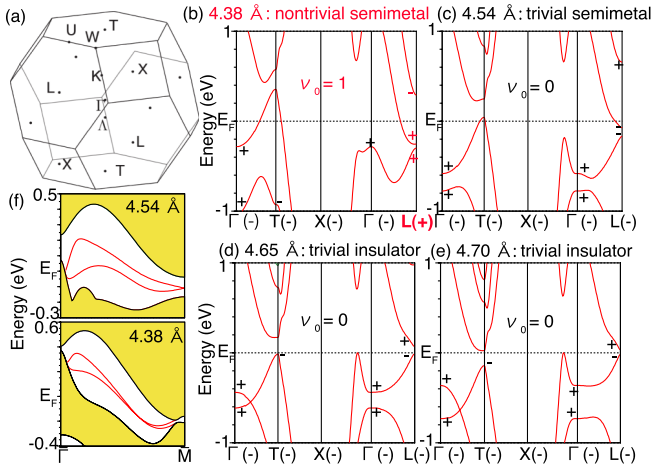

FIG. 4 (color online). (a) Bulk Brillouin zone of Bi. [(b)–(e)] Bulk band structure of Bi with different in-plane lattice constants of (b) 4.38 Å, (c) 4.54 Å, (d) 4.65 Å, and (e) 4.70 Å. The total parity at the Γ and T, X, and L points is shown at the horizontal axis. (f) Surface-state band dispersion by the transfer-matrix tight-binding model for the in-plane lattice constants of 4.54 and 4.38 Å.

Since the contraction of the in-plane lattice constant makes Bi more metallic, expanding it should make it insulating. As shown in Figs. 4(d) and 4(e), Bi does become an insulator with a band gap of ~0.1 eV for in-plane lattice constants of 4.65 and 4.70 Å, respectively. However, the parity analysis suggests that there is no band inversion and that it remains trivial (trivial insulator). Nevertheless, we have found that it is possible to induce several topologically or electronically distinct phases by only a slight lattice distortion in Bi.

In conclusion, we have shown that ultrathin Bi(111) films can be grown on Bi_2Te_3(111), horizontally contracted and vertically expanded compared with the bulk values. Our ARPES study shows that this lattice distortion induces a change in the surface-state band dispersion, and the theoretical calculation reveals that 3D Bi becomes topological, thus offering a novel method to induce topological phases in simple materials.

This work has been supported by Grants-In-Aid from the Japan Society for the Promotion of Science (No. 22656011 and No. 23686007), the JGC-S Scholarship Foundation, the Kao Foundation for Arts and Sciences, and the Support Center for Advanced Telecommunications Technology Research. The ARPES

experiments were performed under the UVSOR Proposal No. 23-515 and No. 24-521. The LEED *I-V* measurements were performed under ISSP Domestic Joint Research No. A223 (2011).

*hirahara@surface.phys.s.u-tokyo.ac.jp

[1] M. Z. Hasan and C. L. Kane, Rev. Mod. Phys. **82**, 3045 (2010).
[2] X.-L. Qi and S.-C. Zhang, Rev. Mod. Phys. **83**, 1057 (2011).
[3] D. Hsieh D. Qian, L. Wray, Y. Xia, Y. S. Hor, R. J. Cava, and M. Z. Hasan, Nature (London) **452**, 970 (2008); Y. Xia *et al.*, Nat. Phys. **5**, 398 (2009).
[4] K. Kuroda *et al.*, Phys. Rev. Lett. **105**, 146801 (2010).
[5] A. A. Taskin, Z. Ren, S. Sasaki, K. Segawa, and Y. Ando, Phys. Rev. Lett. **107**, 016801 (2011).
[6] S. Murakami, Phys. Rev. Lett. **97**, 236805 (2006).
[7] Z. Liu, C-X. Liu, Y.-S. Wu, W.-H. Duan, F. Liu, and J. Wu, Phys. Rev. Lett. **107**, 136805 (2011).
[8] M. S. Bahramy, B.-J. Yang, R. Arita, and N. Nagaosa, Nat. Commun. **3**, 679 (2012).
[9] S. Chadaov, X. Qi, J. Kübler, G. H. Fecher, C. Felser, and S. C. Zhang, Nat. Mater. **9**, 541 (2010).
[10] Y. Sun, X. Q. Chen, S. Yunoki, D. Li, and Y. Li, Phys. Rev. Lett. **105**, 216406 (2010).
[11] T. Sato, K. Segawa, K. Kosaka, S. Souma, K. Nakayama, K. Eto, T. Minami, Y. Ando, and T. Takahashi, Nat. Phys. **7**, 840 (2011).
[12] S.-Y. Xu *et al.*, Science **332**, 560 (2011).
[13] T. Hirahara, T. Nagao, I. Matsuda, G. Bihlmayer, E. Chulkov, Y. Koroteev, P. Echenique, M. Saito, and S. Hasegawa, Phys. Rev. Lett. **97**, 146803 (2006).
[14] T. Shirasawa, M. Ohyama, W. Voegeli, and T. Takahashi, Phys. Rev. B **84**, 075411 (2011).
[15] B.-Y. Li *et al.*, Adv. Mater. **22**, 4002 (2010).
[16] T. Hirahara, G. Bihlmayer, Y. Sakamoto, M. Yamada, H. Miyazaki, S-i. Kimura, S. Blügel, and S. Hasegawa, Phys. Rev. Lett. **107**, 166801 (2011).
[17] T. Nagao, J. Sadowski, M. Saito, S. Yaginuma, Y. Fujikawa, T. Kogure, T. Ohno, Y. Hasegawa, S. Hasegawa, and T. Sakurai, Phys. Rev. Lett. **93**, 105501 (2004).
[18] J. P. Perdew, A. Ruzsinszky, G. Csonka, O. Vydrov, G. Scuseria, L. Constantin, X. Zhou, and K. Burke, Phys. Rev. Lett. **100**, 136406 (2008); Calculations using this exchange-correlation potential more precisely reproduce the experimental lattice constants than those by J. P. Perdew, K. Burke, and M. Ernzerhof, Phys. Rev. Lett. **77**, 3865 (1996).
[19] This feature is also the same in the Bi films formed on Si(111) [T. Hirahara, T. Nagao, I. Matsuda, G. Bihlmayer, E. Chulkov, Y. Koroteev, and S. Hasegawa, Phys. Rev. B **75**, 035422 (2007)]; Furthermore, the drastic difference in the photoemission intensity for bands at different parts of the Brillouin zone has been reported for other systems in relation to the weight spectral function discussed in the following. Refer to D. Topwal, U. Manju, D. Pacilé, M. Papagno, D. Wortmann, G. Bihlmayer, S. Blügel, and C. Carbone, Phys. Rev. B **86**, 085419 (2012) for the case of Au films on Ag(111).
[20] Although (1,0) and (0,1) spots are symmetrically inequivalent in a single crystal, since two rotational domains related to each other by a 180° rotation around the surface normal coexisted in the sample, we have averaged the two LEED spots and employed it as the experimental data. The calculated *I-V* curves are also the average ones.
[21] M. A. V. Hove, W. Moritz, H. Over, P. J. Rous, A. Wander, A. Barbieri, N. Materer, U. Starke, and G. A. Somorjai, Surf. Sci. Rep. **19**, 191 (1993).
[22] Up to 17 phase shifts have been used because of the strong scattering of the heavy Bi atom ($Z = 83$).
[23] H. Mönig, J. Sun, Y. Koroteev, G. Bihlmayer, J. Wells, E. Chulkov, K. Pohl, and P. Hofmann, Phys. Rev. B **72**, 085410 (2005).
[24] T. Shirasawa *et al.* (to be published).
[25] See Supplemental Material at http://link.aps.org/supplemental/10.1103/PhysRevLett.109.227401 for supplemental data.
[26] Note that in ARPES, there is also the matrix element effect of the photoexcitation process and to achieve a complete agreement between the theory and the ARPES image is beyond the scope of the present work.
[27] L. Fu and C. L. Kane, Phys. Rev. B **76**, 045302 (2007).
[28] J. C. Y. Teo, L. Fu, and C. L. Kane, Phys. Rev. B **78**, 045426 (2008).
[29] H.-T. He, G. Wang, T. Zhang, I.-K. Sou, G. Wong, J.-N. Wang, H.-Z. Lu, S.-Q. Shen, and F.-C. Zhang, Phys. Rev. Lett. **106**, 166805 (2011).
[30] J. Seo, P. Roushan, H. Beidenkopf, Y. S. Hor, R. J. Cava, and A. Yazdani, Nature (London) **466**, 343 (2010).